UNIVERSIDADE ESTADUAL DE CAMPINAS
SISTEMA DE BIBLIOTECAS DA UNICAMP
REPOSITÓRIO DA PRODUÇÃO CIENTIFICA E INTELECTUAL DA UNICAMP

Versão do arquivo anexado / Version of attached file:

Versão do Editor / Published Version

Mais informações no site da editora / Further information on publisher's website:
https://iopscience.iop.org/article/10.1088/2050-6120/aa716f

DOI: 10.1088/2050-6120/aa716f

Direitos autorais / Publisher's copyright statement:
©2017 by IOP Publishing. All rights reserved.

DIRETORIA DE TRATAMENTO DA INFORMAÇÃO

Cidade Universitária Zeferino Vaz Barão Geraldo
CEP 13083-970 – Campinas SP
Fone: (19) 3521-6493
http://www.repositorio.unicamp.br

Methods and Applications in Fluorescence

PAPER

RECEIVED
29 October 2016

REVISED
24 April 2017

ACCEPTED FOR PUBLICATION
5 May 2017

PUBLISHED
25 May 2017

Temperature probing and emission color tuning by morphology and size control of upconverting β-$NaYb_{0.67}Gd_{0.30}F_4$:$Tm_{0.015}$:$Ho_{0.015}$ nanoparticles

Emille M Rodrigues, Diogo A Gálico, Italo O Mazali and Fernando A Sigoli

Laboratory of Functional Materials—Institute of Chemistry—University of Campinas—UNICAMP, Campinas, Sao Paulo, PO Box 6154, 13083-970, Brazil

E-mail: fsigoli@iqm.unicamp.br

Keywords: upconversion, nanoparticles, lanthanide fluoride, nanothermometry, White light

Supplementary material for this article is available online

Abstract

The chemical composition, shape and size of upconverting nanoparticles are known to have a great influence on their spectroscopic properties, such as the emission color and the emission intensity variation as a function of temperature. This work shows the color tuning and the thermal sensitivity of $NaYb_{0.67}Gd_{0.30}F_4$:$Tm_{0.015}$:$Ho_{0.015}$ nanoparticles synthesized by two different approaches of the same synthetic method showing the influence of size and morphology, 250 nm hexagonal-plated and 30 nm spheroidal nanoparticles, on the visible upconversion color under NIR irradiation. According to the 1931-CIE diagram, the hexagonal-shaped nanoparticles show white light emission and the spheroidal ones generate red light emission under 980 nm excitation. Besides, the variation of the luminescence intensity ratio of Tm^{3+} emissions as a function of temperature was monitored in the 77–293 K temperature range, and the maximum relative sensitivity (S_m) of the samples reached 1.33% K^{-1} for the hexagonal-plated nanoparticles and 1.76% K^{-1} for the spheroidal nanoparticles. These maximum sensitivity values are higher compared to the ones found in the literature for temperature sensing using upconverting nanoparticles. These data suggest the versatility of these nanoparticles for applications on white light emission and nanothermometry.

Introduction

Lanthanide-doped upconverting nanoparticles (Ln-UCNP) are materials that convert low energy photons in the NIR region into higher energy photons int the UV-visible range. This emission process was first discovered by Auzel [1] in 1966 and has been very useful in materials science. The high tissue penetration of NIR excitation makes it possible for applications in bioimaging [2], indirect excitation of photosensitizers in photodynamic therapies [3], nanothermometry [4] and so on [5]. Many other uses besides the ones related to nanomedicine are also possible, such as applications in solar cells [6] and white light emitting devices [7]. The potential applications normally require the control of synthesis parameters and photophysical properties of these materials. The resulting UV-visible emission after NIR excitation of these materials makes them very attractive for biological applications, such as theranostics. Due to the high absorption coefficient of the Yb^{3+} ion at the NIR region, specifically at 980 nm, many studies regarding Yb^{3+}-doped nanoparticles have been published in the past years [7–10]. Chen *et al* [8] found that similar sized upconverting $NaYbF_4$ nanoparticles are more efficient than the most common $NaYF_4$ host matrix due to the higher absorption cross-section of Yb^{3+} ion at 980 nm. It is also known that the hexagonal (β) crystalline phase of these fluorides systems show higher intensity of upconversion emission bands than the cubic (α) one, because of the lower symmetry of Ln^{3+} which is located in the hexagonal phase C_3 and C_{3h} sites than the symmetric cubic phase O_h site. Besides that, in the hexagonal phase, the distance between Ln^{3+} neighbor ions is shorter than in the cubic phase, favoring the energy transfer mechanisms that normally happens during upconversion processes [8].

The high intensity of upconversion emission is very important for applications of these materials as

© 2017 IOP Publishing Ltd

non-contact temperature probing. It is possible to monitor the intensity ratio between two emission bands [5] and even the emission lifetime [9] of different lanthanide-doped matrices as a temperature function. Thermal sensing using upconversion emitting nanoparticles have been extensively studied, mainly using $NaYF_4$ nanoparticles doped with Er^{3+}, Tm^{3+}, Ho^{3+} and also Nd^{3+} ions using Yb^{3+} as the sensitizer ion [10, 11]. It has been noted that the use of the intensity ratio of two emission bands is one of the most attractive strategies, as it provides a self-referencing system that has a low influence on the excitation intensity or other external parameters [12]. As the ratio variation between the upconversion emission bands depends on non-radiative processes, the size, shape and consequently the surface to volume ratio of the nanoparticles have a significant influence on the temperature sensitivity. Li *et al* [13] found that between $NaYF_4$:Er:Yb nanowires, nanorods and nanoplates shaped nanoparticles, the last ones have a higher temperature sensitivity than the other morphologies, reaching 0.45% K^{-1} at 390 K, due to its higher surface to volume ratio. The type of host matrix and the doping Ln^{3+} ion are also important for the preparation of nanothermometers presenting high thermal sensitivities. In order to achieve that, host matrices where the trivalent lanthanide ions are located in low symmetric chemical environments, such as β-$NaYbF_4$, allow the electronic population of their hypersensitive transitions to be very dependent on temperature, increasing the thermal sensitivity of these potential nanothermometers [5].

However, the synthesis of β-$NaYbF_4$ is not a straightforward task, as the Yb^{3+} ion tends to crystallize the system in the α-cubic phase [14]. Ln^{3+} doping with lighter lanthanides may drive the crystallization of $NaYbF_4$ nanoparticles as the β-hexagonal phase. Using this approach, Damasco *et al* [2] claims to be the first to synthesize Gd^{3+}-doped $NaYbF_4$ nanoparticles in pure hexagonal β-phase. One way to synthesize fluoride nanoparticles is to use the Ostwald-ripening method, where there is the formation of small nuclei at low temperature followed by the Ostwald ripening at higher temperatures [15]. Changes in the electron–phonon coupling at the local crystal field of Ln^{3+}-doped β-$NaYF_4$ systems and ion–ion interactions, allow that band intensities and emission lifetime of doping ion to be directly influenced by environmental temperature variation and by their composition and crystalline phases [8].

This work shows the color tuning and the thermal sensitivity of $NaYb_{0.67}Gd_{0.30}F_4$:$Tm_{0.015}$:$Ho_{0.015}$ nanoparticles synthesized by two different approaches of the same synthetic methodology, illustrating the influence of the nanoparticles size and morphology on the visible upconversion color output under NIR irradiation. According to the 1931-CIE diagram, the hexagonal-shaped nanoparticles show white light emission and spheroidal nanoparticles generate red light emission under 980 nm excitation. Moreover, the variation of the luminescence intensity ratio (LIR) of Tm^{3+} emission bands as a function of temperature was monitored in the 77–293 K temperature range showing one of the highest maximum temperature sensitivities (S_m) among similar known systems.

Experimental

The $NaYb_{0.67}Gd_{0.30}F_4$:$Tm_{0.015}$:$Ho_{0.015}$ nanoparticles synthesis were based on the thermal decomposition method in high boiling point solvents, that is well described in the literature [15]. Briefly, aqueous stock solutions of $YbCl_3$ (0.210 mol l^{-1}), $GdCl_3$ (0.212 mol l^{-1}), $TmCl_3$ (0.110 mol l^{-1}) and $HoCl_3$ (0.094 mol l^{-1}) were used as Ln^{3+} precursors. The preparation of these solutions is described elsewhere [16]. In a 250 ml round botton flask, 3.19 ml of $YbCl_3$, 1.42 ml of $GdCl_3$, 0.14 ml of $TmCl_3$ and 0.16 ml of $HoCl_3$ solutions were added with 3 ml of Oleic Acid (Aldrich, 90%) and 17 ml of 1-Octadecene (Aldrich, 90%). The mixture was heated to 100 °C under N_2 flux and magnetic stirring until complete evaporation of water. Then, the system was closed under a gentle flow of N_2 and the temperature was set to reach 160 °C. After 30 min at 160 °C, the reaction was cooled down to room temperature or 50 °C. At this moment, 10 ml of a 0.4 mol l^{-1} NH_4F and 1 ml of 1 mol l^{-1} NaOH methanol solutions were added to the vessel and the reaction was left under magnetic stirring at the chosen temperature (room temperature or 50 °C) for 30 min. The visual aspect of the solutions at room temperature and 50 °C after the addition of NH_4F and NaOH methanol solutions is shown in figure S1 of the electronic supplementary information (ESI), available at stacks.iop.org/MAF/5/024012/mmedia. Methanol was evaporated under vacuum and the reaction temperature was raised to 300 °C. The synthesis was kept at this temperature for 90 min. The nanoparticles in the powder form were obtained after centrifugation at 9000 rpm for 5 min and washing several times with ethanol.

The XRD patterns were obtained in a Shimatzu XRD 7000 difractometer using CuKα radiation (1.5418 Å). The TEM images were obtained in a Libra —Zeiss transmission electron microscope operating with a tungsten filament at 120 keV. The EDS spectra were obtained in a scanning electron microscope JSM-6360 LV—JEOL operating at 20 kV using as the detector the Noran System SIX, from Thermo Electron Coorporation. The semi-quantitative analysis of the samples composition was made using the method Filter Without Standard of the equipment software, using the System-SIX as an internal reference. The luminescence spectra was obtained in a Fluorolog-3 (Horiba FL3-22-iHR320) spectrofluorimeter with double emission monochomator gratings (1200 gr mm^{-1}, blazed in 500 nm). The upconversion luminescence spectra at room temperature was obtained using a 980 nm CW laser with adjustable power (Crystalaser DL980-1WT$_0$).

In order to evaluate the influence of particle morphologies on the upconverting emission intensities, the spectra were measured using a Quanta-φ (Horiba F-309) integrating sphere equipped with an optical fibers bundle (NA = 0.22–Horiba-FL-3000/FM4-3000) used to guide the UC emission. The 980 nm laser (330 mW) used as an excitation source was straight aligned into the sphere without using the fiber bundle.

For the study of the upconversion emission intensity with variable power, the laser beam was focused on the sample using a convergent lens. The temperature-dependent luminescence spectra of the powder samples were obtained using a cryostat (Janis Research Company VNF-100) coupled to the spectrofluorimeter at the 77–293 K temperature range with a temperature step of 10 K and 15 min of stabilization at each temperature, using the 980 nm laser focused on the powder sample located inside of quartz cell windows with an optical path of 0.1 mm. The laser power was turned on only during the spectra acquisition, in order to avoid any possible sample heating by the laser on the focal spot. All emission spectra at the range of 300 to 750 nm and were corrected according to the optical system and the photomultiplier tube (Hamamatsu R928P).

Results and discussion

$NaLnF_4$ nanoparticles are known to crystallize into cubic (α) or hexagonal (β) phases [14]. The type of precursors used in the synthesis, temperature of nanoparticles formation, the relative amount of sodium ions and Ln precursors added to the synthesis and even the ionic radii of the Ln^{3+} ion used in the host matrix are some of the several factors that may drive the nanoparticles growth into one of the crystalline phases [17, 18]. The Ln^{3+} ions that possesses the higher ionic radii, from La^{3+} to Gd^{3+} tend to crystallize into the β-phase while the ones with smaller radii, from Tb^{3+} to Lu^{3+} normally crystallize as α-phase. Due to the relative disorder of the cation symmetry sites and the low phonon energy, the β-phase of $NaLnF_4$ is considered as the best host matrix for Ln^{3+} upconversion [8]. The $NaYbF_4$ host matrix in the pure hexagonal phase is interesting for high upconversion luminescence intensity due to the major concentration of the 980 nm absorbing Yb^{3+} ion. Wang *et al* [19] used the approach of Gd^{3+}-doping to obtain phase-pure β-$NaYF_4$ nanoparticles with small particle sizes. Lately, some works have been published [20, 21] showing the control over the crystalline phase and nanoparticles morphology by lanthanide doping. In this work, the nanoparticles composition was kept constant and two different temperatures during the NaOH and NH_4F addition step was used. When the addition is made at room temperature, the NaOH and NH_4F solubilities are lower than when this step occurs at 50 °C. Hudry *et al* [22] studied the formation mechanism of the $NaGdF_4$ nanoparticles for this synthetic method and found out that NaF is formed right after the injection of NaOH and NH_4F solutions. The first organized $NaGdF_4$ clusters are formed only after the heating step at 50 °C. The same behavior was observed in this work. When the NaOH and NH_4F solutions are added at room temperature, the low solubility of NaF in the organic solvents results in a turbid suspension, while the heating to 50 °C results in a clear solution containing the first clusters that will grow into the $NaYbF_4$ nanoparticles (ESI—figure S1). Using this synthetic method, the growth of nanoparticles occurs by an Ostwald ripening process, where the larger particles are formed in expense of smaller particles dissolution. Keeping the NaOH and NH_4F addition at room temperature resulted in the formation of larger nuclei that leaded to larger nanoparticles, while the formation of smaller nuclei by the NaOH and NH_4F addition at 50 °C give rise to smaller nanoparticles. TEM images (figure 1) shows the morphology of the final resulting nanoparticles using different temperatures for sodium and fluoride precursors addition.

Besides the different nanoparticle sizes, one may observe that the nanoparticles morphology is also completely different depending on the temperature of sodium and fluoride addition (figure 1). When the addition is performed at room temperature (figure 1(a)), the resulting nanoparticles are hexagonal-plated with 250 nm size and 55 nm thickness. On the other side, when this addition step occurs at 50 °C (figure 1(b)) most of the nanoparticles are spheroidal and some larger nanoparticles with non-defined morphology are also observed. Therefore, besides the chemical compositions of the nanoparticles, the temperature of the sodium and fluoride addition step also plays an important role on controlling the nanoparticles morphology and size.

In order to obtain information regarding the samples composition, the EDS analysis data is shown in table 1. The nominal compositions of the UCNP are similar to the ones found by the EDS semi-quantitative analysis. These results indicate that the differences on the synthetic methodology have just influenced the size and morphology of nanoparticles.

In order to drive the formation of the pure β-hexagonal phase, Gd^{3+} ion was used as a strategy proposed by Wang *et al* [19]. The powder XRD diffractograms of the $NaYb_{0.67}Gd_{0.30}F_4$:$Tm_{0.015}$:$Ho_{0.015}$ nanoparticles (figure 2) indicate that the nanoparticles have pure β-hexagonal phase-P6 space group (JCPDS-PDF: 27–1427) regardless of the temperature of sodium and fluoride addition.

The upconversion (UC) luminescence spectra of the synthesized powder nanoparticles obtained with excitation at 980 nm are shown in figure 3. The UC spectra were obtained without focusing the excitation laser beam on the sample and shows the upconversion emission bands in the visible range attributed to the

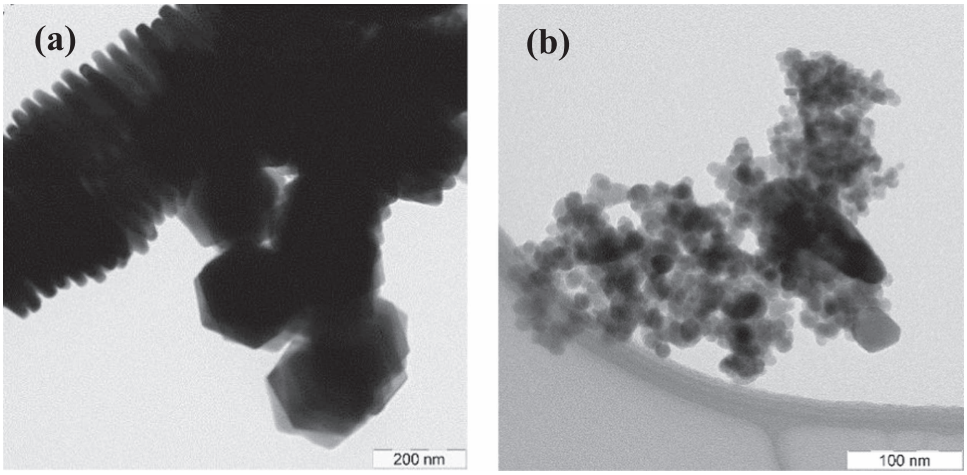

Figure 1. TEM images of the nanoparticles $NaYb_{0.67}Gd_{0.30}F_4$:$Tm_{0.015}$:$Ho_{0.015}$ nucleated at: (a) room temperature and (b) 50 °C.

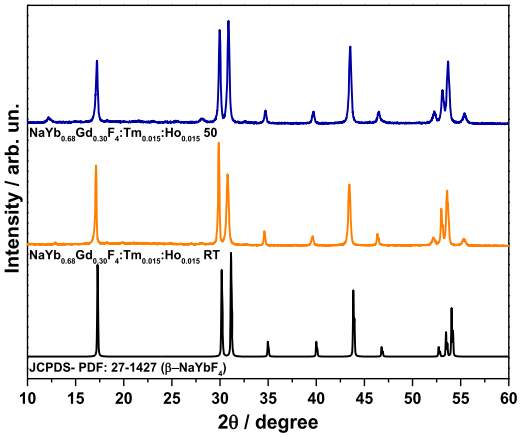

Figure 2. XRD diffraction patterns of the $NaYb_{0.67}Gd_{0.30}F_4$:$Tm_{0.015}$:$Ho_{0.015}$ nanoparticles.

Table 1. Elements nominal and EDS molar ratio of the samples.

	$NaYb_{0.67}Gd_{0.30}F_4$: $Tm_{0.015}$:$Ho_{0.015}$ RT		$NaYb_{0.67}Gd_{0.30}F_4$: $Tm_{0.015}$:$Ho_{0.015}$50	
Elements	Nominal	EDS	Nominal	EDS
Na	1.000	1.000	1.000	1.000
Yb	0.670	0.680	0.670	0.730
Gd	0.300	0.340	0.300	0.330
Tm	0.015	0.023	0.015	0.015
Ho	0.015	0.009	0.015	0.012
F	4.000	4.460	4.000	4.970

Tm^{3+} and Ho^{3+} ions. These emission measurements of both samples were performed on the same day, using powder samples in quartz windows (0.1 mm optical path). The samples position in the sample holder, laser power, excitation and emission slits, integration time, wavelength variation step and the optical geometry were kept the same. The UC emission spectra obtained using an integration sphere (figure 3(b)) confirm that UC emission intensity of the $NaYb_{0.67}Gd_{0.30}F_4$:$Tm_{0.015}$:$Ho_{0.015}$ RT sample is higher than $NaYb_{0.67}Gd_{0.30}F_4$:$Tm_{0.015}$:$Ho_{0.015}$50 one.

Both samples are crystallized as pure β-hexagonal phase and have similar chemical compositions having very different size and morphology (figure 1). The sample $NaYb_{0.67}Gd_{0.30}F_4$:$Tm_{0.015}$:$Ho_{0.015}$ RT, is composed by larger well-defined hexagonal-shaped nanoparticles, while the sample $NaYb_{0.67}Gd_{0.30}F_4$:$Tm_{0.015}$:$Ho_{0.015}$50 is composed by smaller spheroidal nanoparticles with a higher surface-to-volume ratio. Because of the high surface-to-volume ratio, the surface defects became very important, leading to alternative non-radiative decay paths, resulting in low intensity of the upconversion emission from the emitting ions located at the nanoparticles surface. This is a common drawback of very small luminescent nanoparticles, especially the ones where the Yb^{3+} ion is the major lanthanide component of the host matrix. The Yb^{3+} two-level energy results in a faster energy migration through the entire host matrix, leading to high energy transfer rates from ytterbium to thulium and holmium ions located at the nanoparticles surface. As the emission of the surface ions are more affected by the influence of the non-radiative decay routes, for smaller nanoparticles with higher surface to volume ratio, it is expected that there be a decrease of the emission intensities. Using the naked-eye, we observe the upconversion luminescence of the samples, it can clearly be noted that the sample $NaYb_{0.67}Gd_{0.30}F_4$:$Tm_{0.015}$:$Ho_{0.015}$ RT has a white emission while the sample $NaYb_{0.67}Gd_{0.30}F_4$:$Tm_{0.015}$:$Ho_{0.015}$50 has a reddish upconversion luminescence (figure 4). This observation is coherent with the lower intensity of the transitions in the blue and green regions of the spectra for the $NaYb_{0.67}Gd_{0.30}F_4$:$Tm_{0.015}$:$Ho_{0.015}$50 compared to ones on the red region (figure 3). The CIE coordinates of the samples are given in a CIE cromaticity diagram (ESI—figure S2). The pure white coordinates are $x = 0.33$ and $y = 0.33$, and for the $NaYb_{0.67}Gd_{0.30}F_4$:$Tm_{0.015}$:$Ho_{0.015}$RT sample the CIE coordinates are

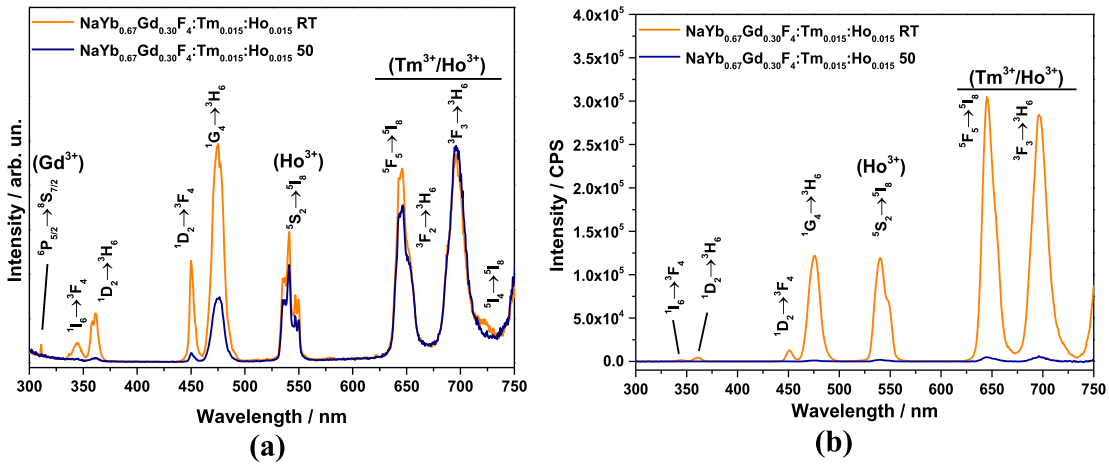

Figure 3. Upconversion emission spectra of the $NaYb_{0.67}Gd_{0.30}F_4$:$Tm_{0.015}$:$Ho_{0.015}$ nanoparticles obtained (a) in the sample powder compartment focusing the laser beam (100 mW) on the samples and (b) inside the integrating sphere (330 mW), confirming the higher emission intensities of the $NaYb_{0.67}Gd_{0.30}F_4$:$Tm_{0.015}$:$Ho_{0.015}$ RT sample.

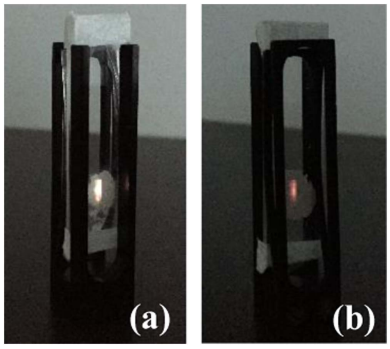

Figure 4. Naked-eye observation of the nanoparticles upconversion luminescence: (a) $NaYb_{0.67}Gd_{0.30}F_4$:$Tm_{0.015}$:$Ho_{0.015}$ RT and (b) $NaYb_{0.67}Gd_{0.30}F_4$:$Tm_{0.015}$:$Ho_{0.015}$50 under 980 nm irradiation at 200 mW without focusing the laser.

x = 0.38 and y = 0.29, that are very close to the white ones. For the $NaYb_{0.67}Gd_{0.30}F_4$:$Tm_{0.015}$:$Ho_{0.015}$50 the color coordinates are x = 0.49 and y = 0.35, close to the red region. It is known that the color tuning of upconverting nanoparticles may be done by changing the chemical composition of lanthanide host matrices, crystalline phases, lanthanide doping and using hierarchical core@shell systems [8]. However, for the present upcoverting nanoparticles, the color tuning was achieved by changing the nanoparticle morphologies leading to different surface to volume ratios and therefore, modifications on non-radiative processes. Figure 5 shows the intensity of the upconversion emission bands as a function of the laser power.

The intensity of the upconversion emission can change with the laser power according to the power law [23], $I = P^n$, where P is the laser power, I is the transition intensity and n the number of absorbed photons for each emitted photon. As it can be seen in figure 6, the number of photons involved in the upconversion emissions for each one of the samples are different. For the sample $NaYb_{0.67}Gd_{0.30}F_4$:$Tm_{0.015}$:$Ho_{0.015}$ RT the n value for every upconversion transition is lower than for the sample $NaYb_{0.67}Gd_{0.30}F_4$:$Tm_{0.015}$:$Ho_{0.015}$50, once again indicating the influence of the nanoparticles surface defects on emission. Based on these results, some upconversion mechanisms are proposed hereafter (figure 7). It is worth noticing that the precise upconversion mechanisms are not in the main scope of this work and the precise determination of the UC mechanisms may be the scope for future work due to their complexity. The qualitative proposal obtained from the power law is used as a guide for one among several possible UC mechanisms.

As mentioned above, for the sample $NaYb_{0.67}Gd_{0.30}F_4$:$Tm_{0.015}$:$Ho_{0.015}$ RT the surface defects are less important than for the sample $NaYb_{0.67}Gd_{0.30}F_4$:$Tm_{0.015}$:$Ho_{0.015}$50. For this reason, the cross relaxation process (CR) and the cooperative energy transfer (CET) mechanisms are viable for this sample, in spite of the very low efficiency of these mechanisms in other upconversion systems [11]. As it can be seen in figure 6(a), the n value can be approximated by 2 for the transitions $^1I_6 \rightarrow {}^3F_4$, $^1D_2 \rightarrow {}^3H_6$, $^1D_2 \rightarrow {}^3F_4$, $^1G_4 \rightarrow {}^3H_6$. As shown in figure 7(a) initially two ytterbium ions may absorb one photon each and through CET the $^1G_4$ level of Tm^{3+} is populated. From this level, the 475 nm $^1G_4 \rightarrow {}^3H_6$ emission occur with $n = 2$. However, a CR can happen populating $^1I_6$ level, resulting into the radiative emission from $^1I_6 \rightarrow {}^3F_4$ at 344 nm with $n = 2$. Another CR may happen and the population of $^1D_2$ level can lead to the emission $^1D_2 \rightarrow {}^3H_6$ at 360 nm and $^1D_2 \rightarrow {}^3F_4$ in 450 nm both with $n = 2$. As for the transitions $^5F_5 \rightarrow {}^5I_8$ and $^3F_3 \rightarrow {}^3H_6$ of Ho^{3+} and Tm^{3+}, respectively, that are very close in energy (figure 5) the n value can be approximate for 1.5, and it can be explained by energy transfer upconversion (ETU) mechanism. After the transfer of two photons from Yb^{3+} to Ho^{3+} and one photon from Yb^{3+} to Tm^{3+} ions, the $^5F_5$ level of Ho^{3+}

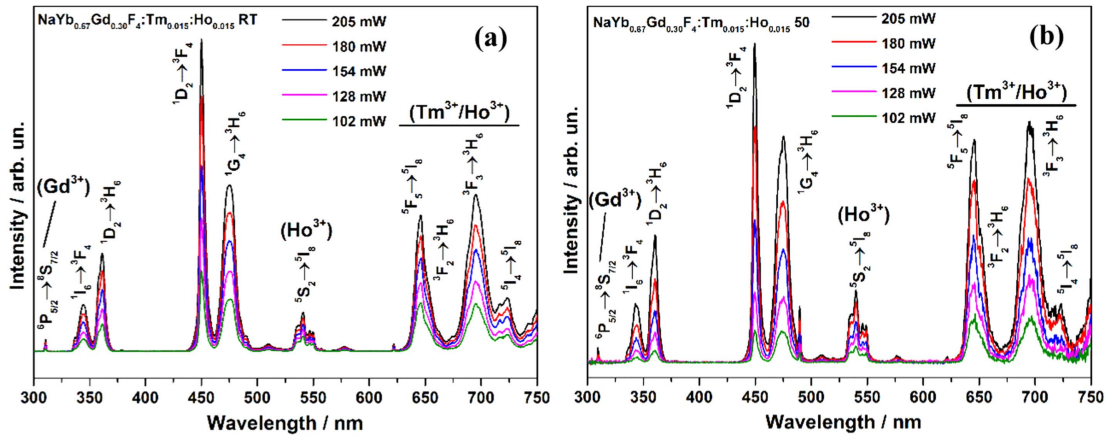

Figure 5. Upconversion emission spectra of the (a) $NaYb_{0.67}Gd_{0.30}F_4$:$Tm_{0.015}$:$Ho_{0.015}$ RT and (b) $NaYb_{0.67}Gd_{0.30}F_4$:$Tm_{0.015}$:$Ho_{0.015}$50 nanoparticles as a function of different 980 nm laser powers. All spectra were obtained with the laser beam focused on the sample.

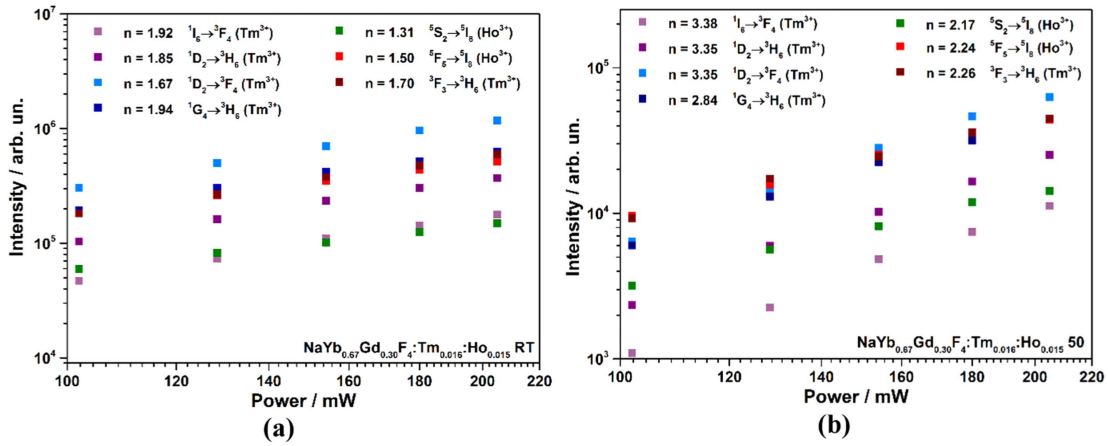

Figure 6. Log-log plots of the upconversion luminescence intensity versus 980 nm laser power of the samples (a) $NaYb_{0.67}Gd_{0.30}F_4$:$Tm_{0.015}$:$Ho_{0.015}$ RT and (b) $NaYb_{0.67}Gd_{0.30}F_4$:$Tm_{0.015}$:$Ho_{0.015}$50.

and $^3H_5$ level of Tm^{3+} are populated and can result into the radiative decay from $^5F_5 \rightarrow {}^5I_8$ at 650 nm. However, simultaneously a CR process can occur, followed by the emission from $^3F_3 \rightarrow {}^3H_6$ of Tm^{3+} near 650 nm. This process may involve the absorption of three photons and the emission of two, resulting in the observed n value of 1.5. For the Ho^{3+} transition $^5S_2 \rightarrow {}^5I_8$ the n value can also be approximated to 1.5, and in figure 7(b) it is shown that the mechanism for this emission also involves Tm^{3+} ions. Through CET between two Yb^{3+} the $^1G_4$ of Tm^{3+} is populated and can transfer the energy to $^3K_8$ of Ho^{3+}. After a non-radiative decay, the 540 nm $^5S_2 \rightarrow {}^5I_8$ emission occurs. Simultaneously another CR takes place and after the transfer of one more photon from Yb^{3+} the Ho^{3+} $^3K_8$ level is once again populated, resulting in the emission of one more photon from $^5S_2 \rightarrow {}^5I_8$. In this proposed mechanism, the absorption of 3 photons on NIR and the emission of 2 photons at 540 nm results in $n = 1.5$ for this transition.

As for the $NaYb_{0.67}Gd_{0.30}F_4$:$Tm_{0.015}$:$Ho_{0.015}$50 sample, figure 6(b) shows $n = 3$ for the $^1I_6 \rightarrow {}^3F_4$, $^1D_2 \rightarrow {}^3H_6$, $^1D_2 \rightarrow {}^3F_4$, $^1G_4 \rightarrow {}^3H_6$ transitions, and the mechanisms proposals for these transitions are given in figure 7(c). Due to the higher surface to volume ratio of the $NaYb_{0.67}Gd_{0.30}F_4$:$Tm_{0.015}$:$Ho_{0.015}$50 sample compared to $NaYb_{0.67}Gd_{0.30}F_4$:$Tm_{0.015}$:$Ho_{0.015}$RT, the CET mechanism is not viable in this case, but CR is still possible. Through ETU, three photons are transferred from Yb^{3+} to Tm^{3+} and $^1G_4$ level is populated, resulting in the $^1G_4 \rightarrow {}^3H_6$ transition at 475 nm with $n = 3$. However a CR can occur populating $^1D_2$ from which $^1D_2 \rightarrow {}^3H_6$, $^1D_2 \rightarrow {}^3F_4$ transitions at 360 and 450 nm occur, respectively with $n = 3$. Another CR can happen populating $^1I_6$ level and the emission $^1I_6 \rightarrow {}^3F_4$ can happen with a $n = 3$. The Tm^{3+} transition $^3F_3 \rightarrow {}^3H_6$ can be explained by ETU of two photons. For Ho^{3+} $^5S_2 \rightarrow {}^5I_8$ transition at 540 nm the excited state absorption (ESA) mechanism explains the $n = 2$ value found for this emission. Similarly, through the ETU mechanism, the 650 nm $^5F_5 \rightarrow {}^5I_8$ transition can be explained.

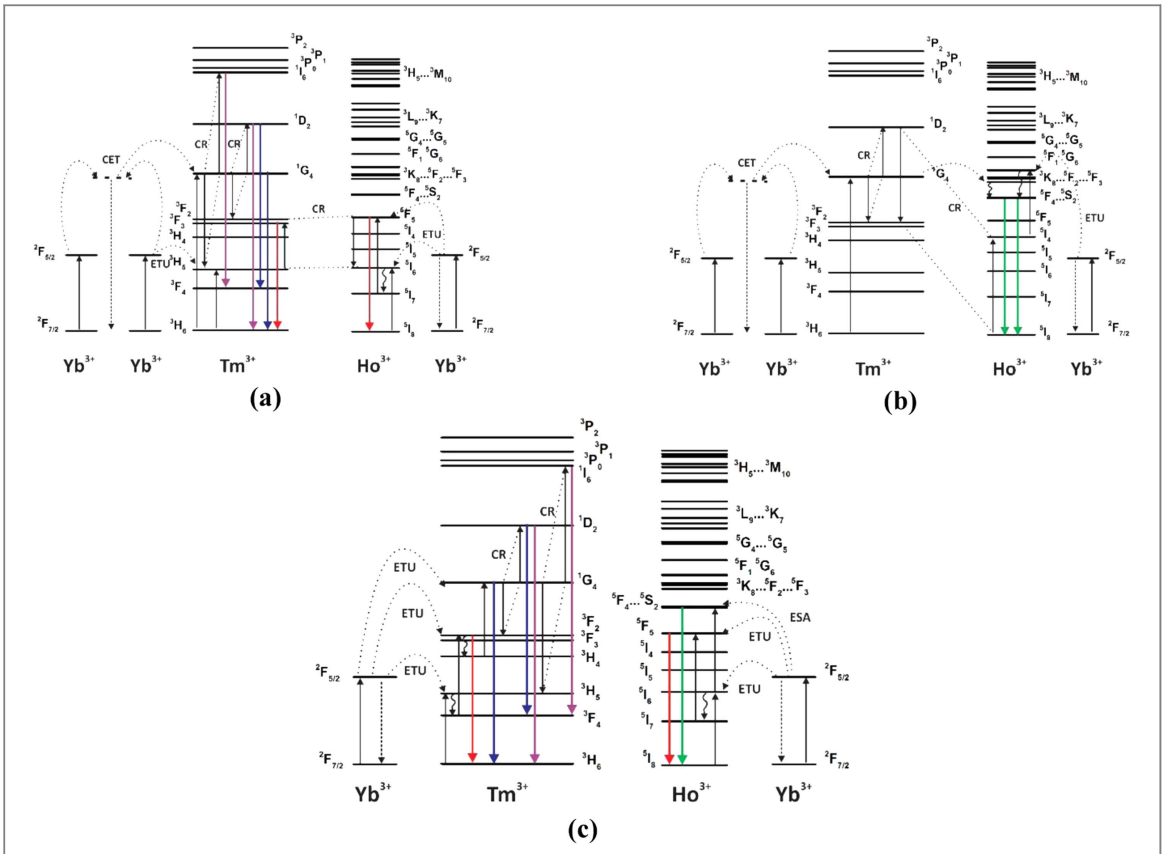

Figure 7. Schematic proposals of upconversion mechanisms: (a) $NaYb_{0.67}Gd_{0.30}F_4$:$Tm_{0.015}$:$Ho_{0.015}$ RT for the $^1I_6 \rightarrow {}^3F_4$, $^1D_2 \rightarrow {}^3H_6$, $^1D_2 \rightarrow {}^3F_4$, $^1G_4 \rightarrow {}^3H_6$, $^5F_5 \rightarrow {}^5I_8$ and $^3F_3 \rightarrow {}^3H_6$ transitions, (b) $NaYb_{0.67}Gd_{0.30}F_4$:$Tm_{0.015}$:$Ho_{0.015}$ RT for $^5S_2 \rightarrow {}^5I_8$ transition and (c) $NaYb_{0.67}Gd_{0.30}F_4$:$Tm_{1.5}$:$Ho_{1.5}$50 for all the upconversion emissions.

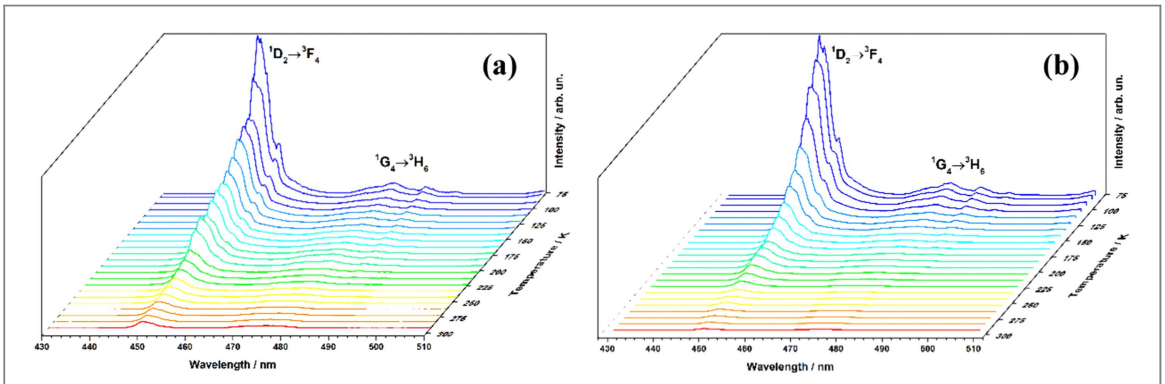

Figure 8. Dependence of the Tm^{3+} upconversion emission intensity as a temperature function showing the variation of Tm^{3+} emissions of: (a) $NaYb_{0.67}Gd_{0.30}F_4$:$Tm_{0.015}$:$Ho_{0.015}$ RT and (b) $NaYb_{0.67}Gd_{0.30}F_4$:$Tm_{0.015}$:$Ho_{0.015}$50 samples.

The measurements of the upconversion emission intensities as a function of the temperature in the 77–273 K range show that the band intensities ratio between the $^1D_2 \rightarrow {}^3F_4$ (450 nm) and $^1G_4 \rightarrow {}^3H_6$ (475 nm) transitions attributed to Tm^{3+} ion greatly changes as a function of the temperature (figure 8).

The LIR between the emission bands attributed to the $^1D_2 \rightarrow {}^3F_4$ and $^1G_4 \rightarrow {}^3H_6$ transitions as a function of the temperature and the relative thermal sensitivity in % K^{-1} were determined as follows:

$$LIR = \frac{I_{450}}{I_{475}} \qquad (1)$$

$$S = \frac{1}{LIR}\left(\frac{dLIR}{dT}\right) \times 100. \qquad (2)$$

Figure 9 shows the plot of LIR and the relative sensitivity of each sample as a function of the temperature. It can be observed that for the sample $NaYb_{0.67}Gd_{0.30}F_4$:$Tm_{0.015}$:$Ho_{0.015}$ RT the maximum relative sensitivity reaches 1.33% K^{-1} at 163 and 203 K and for the sample $NaYb_{0.67}Gd_{0.30}F_4$:$Tm_{0.015}$:$Ho_{0.015}$50, the relative sensitivity reaches the maximum of 1.76% K^{-1} at 183 K. The slightly higher sensitivity of the sample $NaYb_{0.67}Gd_{0.30}F_4$:$Tm_{0.015}$:$Ho_{0.015}$50 compared to the $NaYb_{0.67}Gd_{0.30}F_4$:$Tm_{0.015}$:

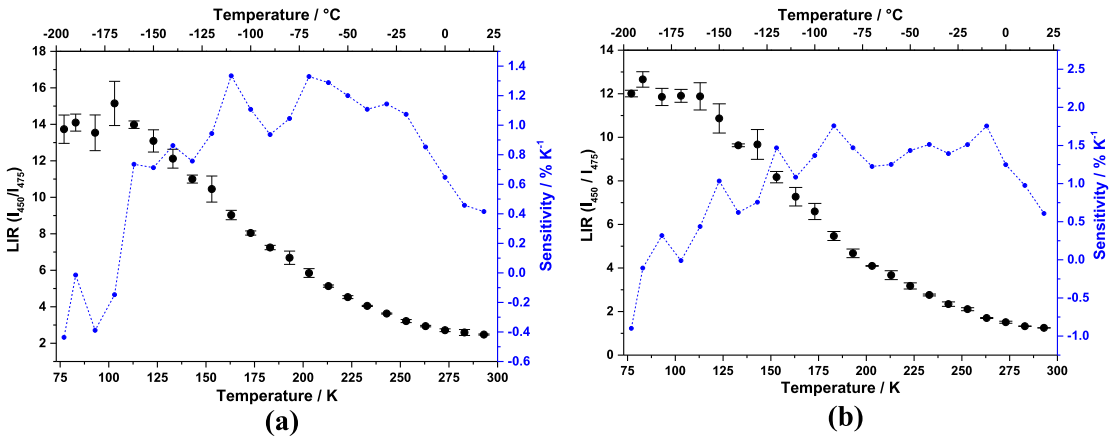

Figure 9. LIR and relative sensitivity in % K^{-1} as a function of the temperature for the nanoparticles:(a) $NaYb_{0.67}Gd_{0.30}F_4$:$Tm_{0.015}$:$Ho_{0.015}$ RT and (b) $NaYb_{0.67}Gd_{0.30}F_4$:$Tm_{0.015}$:$Ho_{0.015}$50.

Table 2. Maximum thermal sensitivity (S_m) and the probing temperature range of some upconverting Ln^{3+}-doped nanomaterials using LIR as figure of merit.

Host materials	Dopant ion—(Used λ-nm)	S_m (% K^{-1})	Temperature Range (K)	Temperature of S_m (K)	References
$NaYbF_4$:Gd:Tm:Ho RT	Tm-(450/475)	1.33	77–293	163 and 203	This work
$NaYbF_4$:Gd:Tm:Ho 50	Tm-(450/475)	1.76	77–293	183	This work
$NaGdF_4$:Yb:Tm/(Tb/Eu)	Tb/Eu-(545/615)	1.20	50–300	125 to300	[24]
$NaYF_4$:Yb:Er	Er-(525/545)	1.20	160–300	300	[25]
$NaYF_4$:Yb:Tm/$NaYF_4$:Pr	Tm-(642/695)	1.53	350–510	417	[26]
Y_2O_3:Yb:Tm	Tm-(476/488)	0.75	303–753	303	[27]
$CaWO_4$:Yb:Ho	Ho-(460/487)	0.50	303–923	923	[28]
ZnO:Er	Er-(530/563)	0.62	273–573	443	[29]
$NaNbO_3$:Yb:Tm	Tm-(480/486)	0.08	293–373	constant at the entire range	[30]

$Ho_{0.015}$ RT is probably due to the smaller size of the former nanoparticles. Smaller sized nanoparticles have a higher surface to volume ratio, which makes the non-radiative process at the nanoparticle surface important. As these processes are responsible for the changes in LIR with the temperature, the $NaYb_{0.67}Gd_{0.30}F_4$:$Tm_{0.015}$:$Ho_{0.015}$50 sample where the non-radiative processes are more relevant has the higher maximum thermal sensitivity.

The values of maximum thermal sensitivity (S_m) for some systems using upconversion emissions for temperature probing are given in table 2. Considering the ratio between upconversion emission bands of just one emitting ion, both samples obtained in this work have higher maximum thermal sensitivity as well as higher relative sensitivity in a wide range of temperatures than the systems shown in table 2. These data suggest the potentiality of these nanoparticles for optical nanothermometry applications. Moreover, these results show that for thermal sensing purposes, smaller nanoparticles may give rise to higher relative thermal sensitivities probably due to high surface to volume ratio and the high lanthanide concentration at the NP surface.

Conclusions

This work showed the synthesis and characterization of β-$NaYb_{0.67}Gd_{0.30}F_4$:$Tm_{0.015}$:$Ho_{0.015}$ nanoparticles with upconversion emission color tuning and potential application on nanothermometry. The main emission intensity differences of the nanoparticles were obtained due the variation of nanoparticles surface to volume ratio leading to non-radiative processes. These observations indicate that the temperature of addition of NaOH and NH_4F solutions during the nanoparticles synthesis plays an important role. The addition at 50 °C resulted in smaller nuclei with non-homogeneous growth and leads to spheroidal nanoparticles with small sizes and orange/red upconversion emission. The addition at room temperature results in larger nuclei leading to hexagonal-plated nanoparticles that show white light upconversion according to CIE diagram, being visible by the naked-eye. The maximum thermal sensitivity of the smaller nanoparticles obtained by the nucleation at 50 °C is slightly higher (1.76% K^{-1}) than the one obtained for the larger particles (1.33% K^{-1}), due to the higher surface

to volume ratio on the smaller ones. Both systems have higher maximum thermal sensitivity as well as higher relative sensitivity at a wide range of temperatures than other systems found in the literature. The results suggest the versatility of these upconverting nanoparticle systems for white light emission and nanothermometry applications.

Acknowledgments

EMR and DAG are indebted to CNPq for the PhD fellowship. IOM and FAS are indebted to INOMAT, CNPq, CAPES and FAPESP (grant: 2013/22127-2) for financial support. The funders had no role in study design, data collection and analysis, decision to publish, or preparation of the manuscript. All authors would like to thank Dr Douglas Soares for the EDS measurements and also the Multiuser Laboratory of Advanced Optical Spectroscopy—Institute of Chemistry-UNICAMP.

The authors have declared that no conflict of interests exist.

References

[1] Auzel F 2004 Upconversion and anti-stokes processes with f and d ions in solids *Chem. Rev.* **104** 139–73

[2] Damasco J A, Chen G, Shao W, Ågren H, Huang H, Song W, Lovell J F and Prasad P N 2015 Size-tunable and monodisperse Tm^{3+}/Gd^{3+}-doped hexagonal $NaYbF_4$ nanoparticles with engineered efficient near infrared-to-near infrared upconversion for *in vivo* Imaging *ACS Appl. Mater. Interfaces* **6** 13884–93

[3] Punjabi A *et al* 2014 Amplifying the red-emission of upconverting nanoparticles for biocompatible clinically used prodrug-induced photodynamic therapy *ACS Nano* **8** 10621–30

[4] Wang X, Zheng J, Xuan Y and Yan X 2013 Optical temperature sensing of $NaYbF_4:Tm^{3+}@SiO_2$ core–shell micro-particles induced by infrared excitation *Opt. Express* **21** 21596–606

[5] González-Béjar M and Pérez-Prieto J 2015 Upconversion luminescent nanoparticles in physical sensing and in monitoring physical processes in biological samples *Methods. Appl. Fluoresc.* **3** 42002

[6] Yuan C, Chen G, Prasad P N, Ohulchanskyy T Y, Ning Z, Tian H, Sun L and Ågren H 2012 Use of colloidal upconversion nanocrystals for energy relay solar cell light harvesting in the near-infrared region *J. Mater. Chem.* **22** 16709–13

[7] Hu M, Ma D, Liu C, Wang J, Zhang Z and Meng L 2016 Intense white emission from a single-upconversion nanoparticle and tunable emission colour with laser power *J. Mater. Chem.* C **4** 6975–81

[8] Chen G, Yang C and Prasad P N 2013 Nanophotonics and nanochemistry: controlling the excitation dynamics for frequency up- and down-conversion in lanthanide-doped nanoparticles *Acc. Chem. Res.* **46** 1474–86

[9] Savchuk O A, Carvajal J J, Pujol M C, Massons J, Haro-González P, Jaque D, Aguiló M and Díaz F 2014 New strategies for luminescence thermometry in the biological range using upconverting nanoparticles *Proc. SPIE* **9129** 91292E

[10] Xu X *et al* 2015 α-$NaYb(Mn)F_4:Er^{3+}/Tm^{3+}@NaYF_4$ UCNPs as 'band-shape' luminescent nanothermometers over a wide temperature range *ACS Appl. Mater. Interfaces* **7** 20813–9

[11] Dong H, Sun L D and Yan C H 2015 Energy transfer in lanthanide upconversion studies for extended optical applications *Chem. Soc. Rev.* **44** 1608–34

[12] Carlos L D and Palacio F 2016 *Thermometry at The Nanoscale: Techniques And Selected Applications* (Cambridge: The Royal Society of Chemistry)

[13] Li D, Shao Q, Dong Y and Jiang J 2013 Thermal sensitivity and stability of $NaYF_4:Yb^{3+}$, Er^{3+} upconversion nanowires, nanorods and nanoplates *Mater. Lett.* **110** 233–6

[14] Ren J, Jia G, Guo Y, Wang A and Xu S 2016 Unraveling morphology and phase control of $NaLnF_4$ upconverting nanocrystals *J. Phys. Chem.* C **120** 1342–51

[15] Li Z and Zhang Y 2008 An efficient and user-friendly method for the synthesis of hexagonal-phase $NaYF_4$:Yb,Er/Tm nanocrystals with controllable shape and upconversion fluorescence *Nanotechnology* **19** 345606

[16] Rodrigues E M, Souza E R, Monteiro J H S K, Gaspar R D L, Mazali I O and Sigoli F A 2012 Non-stabilized europium-doped lanthanum oxyfluoride and fluoride nanoparticles well dispersed in thin silica films *J. Mater. Chem.* **22** 24109

[17] Thoma R E, Insley H and Hebert M 1966 The sodium fluoride-lanthanide trifluoride systems *Inorg. Chem.* **5** 1222–9

[18] Fedorov P P, Luginina A A, Kuznetsov S V and Osiko V V 2011 Nanofluorides *J. Fluor. Chem.* **132** 1012–39

[19] Wang F, Han Y, Lim C S, Lu Y, Wang J, Xu J, Chen H, Zhang C, Hong M and Liu X 2010 Simultaneous phase and size control of upconversion nanocrystals through lanthanide doping *Nature* **463** 1061–5

[20] Zeng S, Ren G, Xu C and Yang Q 2011 Modifying crystal phase, shape, size, optical and magnetic properties of monodispersed multifunctional $NaYbF_4$ nanocrystals through lanthanide doping *Cryst. Eng. Comm.* **13** 4276–81

[21] Hao S, Shao W, Qiu H, Shang Y, Fan R, Guo X, Zhao L, Chen G and Yang C 2014 Tuning the size and upconversion emission of $NaYF_4:Yb^{3+}/Pr^{3+}$ nanoparticles through Yb^{3+} doping *RSC Adv.* **4** 56302–6

[22] Hudry D, Abeykoon A M M, Dooryhee E, Nykypanchuk D and Dickerson J H 2016 Probing the crystal structure and formation mechanism of lanthanide-doped upconverting nanocrystals *Chem. Mater.* **28** 8752–63

[23] Pollnau M, Gamelin D R, Lüthi S R, Güdel H U and Hehlen M P 2000 Power dependence of upconversion luminescence in lanthanide and transition-metal-ion systems *Phys. Rev.* B **61** 3337–46

[24] Zheng S, Chen W, Tan D, Zhou J, Guo Q, Jiang W, Xu C, Liu X and Qiu J 2014 Lanthanide-doped $NaGdF_4$ core–shell nanoparticles for non-contact self-referencing temperature sensors *Nanoscale* **6** 5675–9

[25] Zhou S, Deng K, Wei X, Jiang G, Duan C, Chen Y and Yin M 2013 Upconversion luminescence of $NaYF_4:Yb^{3+}$,Er^{3+} for temperature sensing *Opt. Commun.* **291** 138–42

[26] Zhou S, Jiang G, Li X, Jiang S, Wei X, Chen Y, Yin M and Duan C 2014 Strategy for thermometry via Tm^{3+}-doped $NaYF_4$ core—shell nanoparticles *Opt. Letters* **39** 6687–90

[27] Li D, Wang Y, Zhang X, Yang K, Liu L and Song Y 2012 Optical temperature sensor through infrared excited blue upconversion emission in Tm^{3+}/Yb^{3+} codoped Y_2O_3 *Opt. Commun.* **285** 1925–8

[28] Xu W, Zhao H, Li Y, Zheng L, Zhang Z and Cao W 2013 Optical temperature sensing through the upconversion luminescence from Ho^{3+}/Yb^{3+} codoped $CaWO_4$ *Sensors Actuators, B Chem.* **188** 1096–100

[29] Wang X, Kong X, Yu Y, Sun Y and Zhang H 2007 Effect of annealing on upconversion luminescence of $ZnO:Er^{3+}$ nanocrystals and high thermal sensitivity *J. Phys. Chem.* C **111** 15119–24

[30] Pereira A F, Kumar K U, Silva W F, Santos W Q, Jaque D and Jacinto C 2015 Yb^{3+}/Tm^{3+} co-doped $NaNbO_3$ nanocrystals as three-photon-excited luminescent nanothermometers *Sensors Actuators, B Chem.* **213** 65–71